

Improving unmanned armoured mobile robot navigation accuracy using Kalman filter

Tanya Porang, Dechrit Maneetham, Padma Nyoman Crisnapati

Department of Mechatronics Engineering, Rajamangala University of Technology Thanyaburi, Khlong Hok, Thailand

Article Info

Article history:

Received May 23, 2024

Revised Oct 5, 2024

Accepted Oct 8, 2024

Keywords:

Armoured mobile robot

Kalman filter

Military robotics

Navigation

Waypoint

ABSTRACT

Thailand's remarkable economic progress has earned it recognition as a development success story, but terrorism remains a significant threat, particularly in the southern provinces. To effectively combat terrorism, intelligent systems like military robots are being increasingly utilized worldwide, including the development of vision-based robots and unmanned military equipment. The Thai government aligns with this trend by aiming to manufacture military robots, including armored mobile robot (AMR) equipped with cameras for peacekeeping and surveillance purposes. The development of an automatic tank simulation robot control system integrates global position system (GPS) technology, digital compasses, and lidar sensors to enhance efficiency, directional control, and obstacle avoidance. The study investigates the implementation of Kalman filters to enhance the precision of navigation in AMRs used in military contexts. The suggested system combines GPS, Lidar sensors, and digital compasses, utilizing advanced sensor fusion algorithms to improve directional control and obstacle avoidance. The system's usefulness is demonstrated through field tests and simulations, especially in complicated contexts where conventional approaches may face difficulties. The findings help to the progress of military robotics by providing a strong answer for improving navigation accuracy in real-world situations.

This is an open access article under the [CC BY-SA](https://creativecommons.org/licenses/by-sa/4.0/) license.



Corresponding Author:

Dechrit Maneetham

Department of Mechatronics Engineering, Faculty of Technical Education

Rajamangala University of Technology Thanyaburi

Tambon Khlong Hok, Amphoe Thanyaburi Pathum Thani 12110, Thailand

Email: dechrit_m@rmutt.ac.th

1. INTRODUCTION

Over the past forty years, Thailand's economy has grown remarkably, moving the country from a low-income to an upper-middle-income status and garnering praise for its development accomplishments [1]. However, the nation is still facing significant threats from terrorism, particularly in the southern provinces of Yala, Narathiwat, and Pattani [2]. Utilizing cutting-edge equipment, such military robots, has become crucial in addressing these security issues. Unmanned robot technology is developing quickly on a global scale, and many nations are making significant investments in it [3]. By enabling remote or autonomous operations that help to minimize deaths and reduce the need on human troops, these military robots play a critical role in aiding armed forces [4].

In modern defense systems and security operations, the role of armored mobile robots (AMR) is becoming increasingly significant [5]. These vehicles offer a variety of benefits, including reduced risk to personnel, enhanced reconnaissance capabilities and increased operational efficiency [6]. The development of unmanned systems, particularly armored vehicles, has become a focal point in modern defense strategies.

As these systems are deployed in increasingly complex environments, the need for accurate and reliable navigation systems becomes paramount. Previous research has explored various approaches to improve the navigation accuracy of these vehicles, yet challenges remain, particularly in dynamic and obstacle-filled environments. However, ensuring proper AMR navigation and control remains a critical challenge, especially in complex and dynamic environments. Artificial intelligence (AI) has become increasingly important in the defense sector, and organizations are realizing its potential [7]. In line with this trend, the Thai government aims to utilize Industry 4.0 concepts in the defense sector by producing military robots [8]-[10]. Military robots equipped with cameras are being developed to maintain peace and carry out surveillance in conflict zones and along borders. In particular, research on military tank robotic systems has been carried out [11], [12]. One promising approach to overcome this challenge is the application of Kalman filters [13]. Kalman filters are widely used in navigation systems to estimate the state of a dynamic system based on a series of noise measurements [14]-[16]. By integrating data from multiple sensors and refining estimates over time, Kalman filters can significantly improve the accuracy and reliability of navigation [17], [18].

This paper focuses on the simulation, development, and evaluation of a Kalman filter-based AMR navigation system for unmanned armored vehicles. We investigate the effectiveness of the Kalman filter in improving navigation accuracy in various scenarios, including straight-line trajectories, sharp turns, and obstacle-filled environments. The control system design includes features such as controlling the movement of the driverless car via a global position system (GPS) system, digital compass, and lidar sensors to improve directional control and obstacle avoidance [19]-[21]. The significance of this research lies in addressing the gap between existing navigation systems and the requirements for high precision in military applications. While many studies have utilized sensor fusion techniques, the integration of Kalman Filters offers a promising approach to refining navigation accuracy. For instance, studies by [22]-[24] have demonstrated the potential of Kalman Filters in improving state estimation in mobile robots. However, these studies often focused on controlled environments or lacked comprehensive field testing. This paper aims to fill this gap by developing a robust navigation system for AMRs that can operate effectively in real-world scenarios. The research builds on the work of previous contributors but distinguishes itself by its focus on integrating Kalman filters with a combination of GPS, lidar sensors, and digital compasses for enhanced navigation accuracy. The following sections will outline the problem, review relevant literature, and describe the methodology used to address the identified gaps.

AMR operation is facilitated by setting latitude and longitude coordinates on a map and utilizing the Arduino Mega board as the main processor, which works together with the motor control unit, digital compass and GPS module. The system is designed to determine the AMR's position coordinates, transmit the coordinates to the controller, and incorporate obstacle avoidance capabilities for dynamic obstacle avoidance during the mission. Additionally, a compass is integrated to help control the direction of movement of the AMR, ensuring accurate navigation towards the desired destination. By conducting experimental studies and analyzing the results, we aim to demonstrate the potential of Kalman filters to significantly improve the performance of unmanned armored vehicle navigation systems. Through this research, we seek to contribute to the advancement of Thailand's defense capabilities by developing robust and precise navigation solutions for unmanned armored vehicles. The organization of this work is as follows: the subsequent section provides an elaborate methodology section that delineates the design, development, and evaluation of the suggested navigation system. The results section contains empirical observations, which are analyzed in relation to prior research, and the paper finishes with a discussion of implications of this study and recommendations for future research.

2. METHOD

2.1. Mechanical, electronics, and software design

As an initial stage of this research, the mechanical design of the AMR resembles a miniature tank. This mobile robot concept adopts a caterpillar track with several combinations of gears, bearings, struts, coil springs, chains, and two DC motors, as presented in Figure 1. The rear driving wheel is directly connected to the DC motor shaft and serves as the main mover of this robot. The movement of this mobile robot adapts the differential drive system. At this prototype stage, the body, top cover, and caterpillar track of the tank are made of iron. There are two tracks on a caterpillar track vehicle one on each side. These vehicles are widely used in mining, agriculture, defense, and other off-road industries.

2.2. Kinematic model of a tracked vehicle

Kinematic models were developed for the AMR based on the computer aided design (CAD) mechanical design. Because of its superior handling of longitudinal slides, greater traction, and decreased ground compaction, tracked vehicles are becoming more and more common in tough terrain. Their increasing

application in agriculture emphasizes the necessity of precise models for creating controllers that can track paths. The kinematic model of a tracked vehicle is derived in this section and is also relevant to vehicles driven differently. Steering is accomplished by driving the left and right tracks at different speeds, which causes the tracked vehicle to skid. Tracked vehicles have continuous tracks, similar to those found on military tanks. We see this kinematic model in Figure 2.

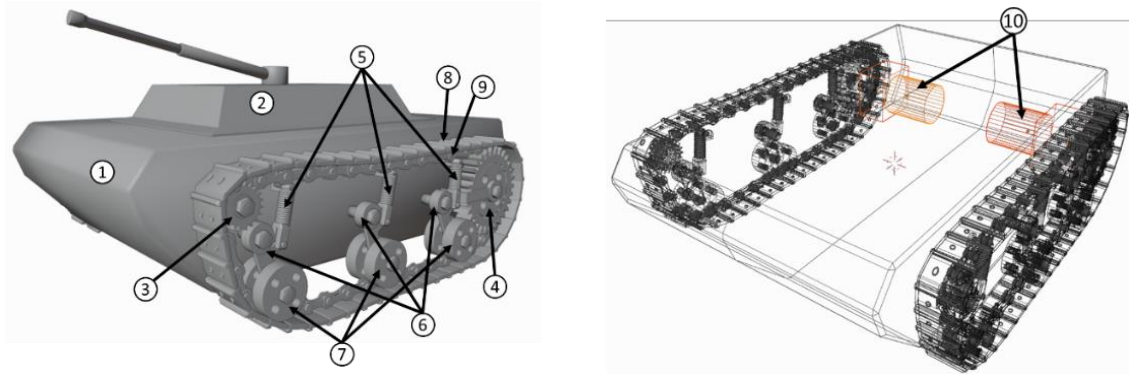


Figure 1. 3D CAD model design that contains of: 1) tank body; 2) tank top cover; 3) bearing wheel; 4) rear driving wheel; 5) coil spring; 6) strut; 7) lower roll; 8) metal track; and 9) metal chain

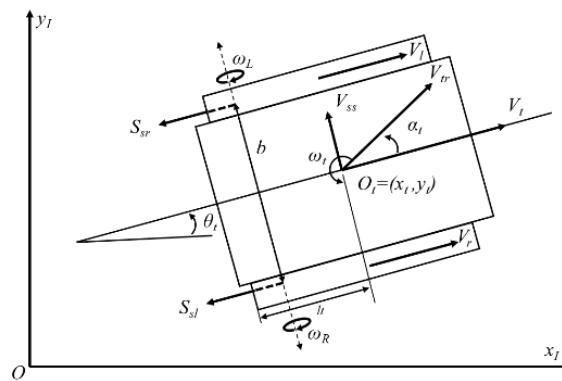


Figure 2. Kinematic model of AMR

The center of mass of the tracked vehicle is where the body-fixed coordinate system is situated [25]. The heading angle in the global coordinate system is denoted by θ_t , while the origin coordinates are x_t and y_t . The tread width of the vehicle is marked as b , while the half-track length is indicated as l [26]. The velocities from the tracks act as control inputs for the vehicle's speed and steering rate in a kinematic model. The tracks also produce driving forces. Similar to wheeled vehicles, tracked vehicles also undergo slippage, which can be modelled by taking longitudinal slip and slip angle into account at each track [27]. There are no lateral forces when the vehicle's motion direction is in line with the track motion direction. However, when the travel direction changes as a result of obstructions or uneven [28]. Table 1 provides a comprehensive summary of the kinematic model.

Table 1. Equation definition

Nomenclature					
O_t :	tank Origin	l :	half-track length	S_{sr} :	right hand side slip values
x_t :	x coordinate of the tank	b :	vehicle tread	S_{sl} :	left hand side slip values
y_t :	y coordinate of the tank	θ_t :	heading angle	α_t :	side slip angle
V_l :	linear velocity of left wheel	V_r :	linear velocity of right wheel	ω_t :	net angular velocity
V_t :	net longitudinal velocity	V_{ss} :	lateral velocity		

$$\alpha_{st} = \tan^{-1} \left(\frac{V_{ss}}{V_t} \right) \tag{1}$$

$$S_{sr} = 1 - \frac{V_r}{r\omega_r} = \frac{r\omega_r - V_r}{r\omega_r} \quad (2)$$

$$\dot{x}_t = \frac{r}{2} [\omega_l(1 - S_{sl}) + \omega_r(1 - S_{sr})] [\cos \theta_t - \sin \theta_t \tan \alpha_{st}] \quad (3)$$

$$\dot{y}_t = \frac{r}{2} [\omega_l(1 - S_{sl}) + \omega_r(1 - S_{sr})] [\sin \theta_t + \cos \theta_t \tan \alpha_{st}] \quad (4)$$

$$\dot{\theta}_t = \frac{r[\omega_l(1 - S_{sl}) + \omega_r(1 - S_{sr})]}{b} \quad (5)$$

$$\omega_t = \frac{r}{b} (\omega_r - \omega_l) \quad (6)$$

$$V_t = \frac{r}{2} (\omega_r + \omega_l) \quad (7)$$

$$\dot{x}_t = V_t \cos \theta_t + \dot{V}_{dx} \quad (8)$$

$$\dot{y}_t = V_t \sin \theta_t + \dot{V}_{dy} \quad (9)$$

$$\theta_t = \omega_t + \omega_d \quad (10)$$

$$\dot{V}_{dx} = -V_t \sin \theta_t \tan \alpha_{st} - \frac{r}{2} (\omega_r S_{sl} + \omega_l S_{sr}) \cos \theta_t + \frac{r}{2} (\omega_r S_{sl} + \omega_l S_{sr}) \sin \theta_t \tan \alpha_{st} \quad (11)$$

$$\dot{V}_{dy} = -V_t \cos \theta_t \tan \alpha_{st} - \frac{r}{2} (\omega_r S_{sl} + \omega_l S_{sr}) \sin \theta_t + \frac{r}{2} (\omega_r S_{sl} + \omega_l S_{sr}) \cos \theta_t \tan \alpha_{st} \quad (12)$$

$$\omega_d = \frac{r}{b} (\omega_r S_{sl} - \omega_l S_{sr}) \quad (13)$$

The lateral force, acting perpendicular to the vehicle's orientation, uniformly affects the vehicle. The side slip angle α_{st} measures the difference between the vehicle's heading and its actual direction (1), defined using lateral velocity V_{ss} and net longitudinal velocity V_t at the center of gravity. Longitudinal slip values, S_{sl} for the left track and S_{sr} for the right track, are defined separately and may not always correlate. Longitudinal slip (2) [29] can sometimes increase speed, such as when climbing a slope, but usually hinders forward motion. For the right track, longitudinal slip is defined using the linear speed ω_r , driven by the sprocket rotating at angular speed ω_r with a radius r , and net forward speed V_r . The left track's slip s_{sl} is determined similarly [17]. The kinematic model includes α_{st} , S_{sr} , and S_{sl} . To simplify controller design, in (3)-(5) are reformulated using the vehicle's linear and angular velocities, V_t and ω_t , instead of the tracks' angular velocities ω_l and ω_r . The final kinematic equations, incorporating track slips, are presented with relationships between vehicle and track velocities. Vehicle sliding introduces terms V_{dx} , V_{dy} , and ω_d [30].

Figure 3 illustrates the electronics and software design, providing a detailed overview of the system's architecture and functionality. Figure 3(a) wiring diagram illustrates how different electrical components that are essential to a system perhaps an autonomous car or military robot be integrated (1) Raspberry Pi; 2) Arduino Mega; 3) DC motor drivers; 4) Stepdown; 5) Ublox M8N GPS; 6) Compass; 7) MPU6050; 8) Bluetooth; 9) MicroSD card module; 10) YDLidar X4; 11) DC motors; and 12) power supply). These parts include the Arduino Mega and Raspberry Pi microcontroller boards, which handle low-level control and high-level processing, respectively. DC motor drivers control the direction and speed of the DC motors, and a stepdown converter maintains appropriate voltage levels across the system. While the MPU6050 accelerometer and gyroscope provide motion sensing capabilities, modules like the Ublox M8N GPS and compass offer precise positioning and orientation data. Wireless communication is enabled via Bluetooth, and data storage is made possible by a MicroSD card module. The YDLidar X4 Lidar sensor helps in mapping and obstacle detection. A power supply unit provides power to the system, guaranteeing that every part operates as it should. These elements work together to create a unified system that is intended to function well in a variety of navigation, control, and operation settings.

The system flowchart in Figure 3(b) shows the steps involved in operating a mobile robot that can navigate waypoints and avoid obstacles. First, the system sets up necessary parts such as the GPS, compass, Lidar, and inertial measurement unit (IMU). The first navigational waypoint is then retrieved. The system then determines whether there are any waypoints left to route to. In the event that waypoints are still present, the robot's current position and orientation are ascertained by the system using GPS data and the compass direction filtered by Kalman Filter. Lidar data is gathered in tandem to identify any obstructions in the robot's

path. The system starts obstacle avoidance navigation when it detects an obstruction, changing the direction of navigation according to the compass heading. The system checks to see if the current waypoint has been reached if no obstacles are found. After reaching the waypoint, the algorithm looks for other ones. The procedure repeats, retrieving the next waypoint, if there are any more waypoints. After navigating all waypoints, the system shuts off the motors and ends the process. The system continuously calculates the navigation vector during the procedure, directing the robot's movement in accordance with the intended path determined by the waypoints and obstacle avoidance factors.

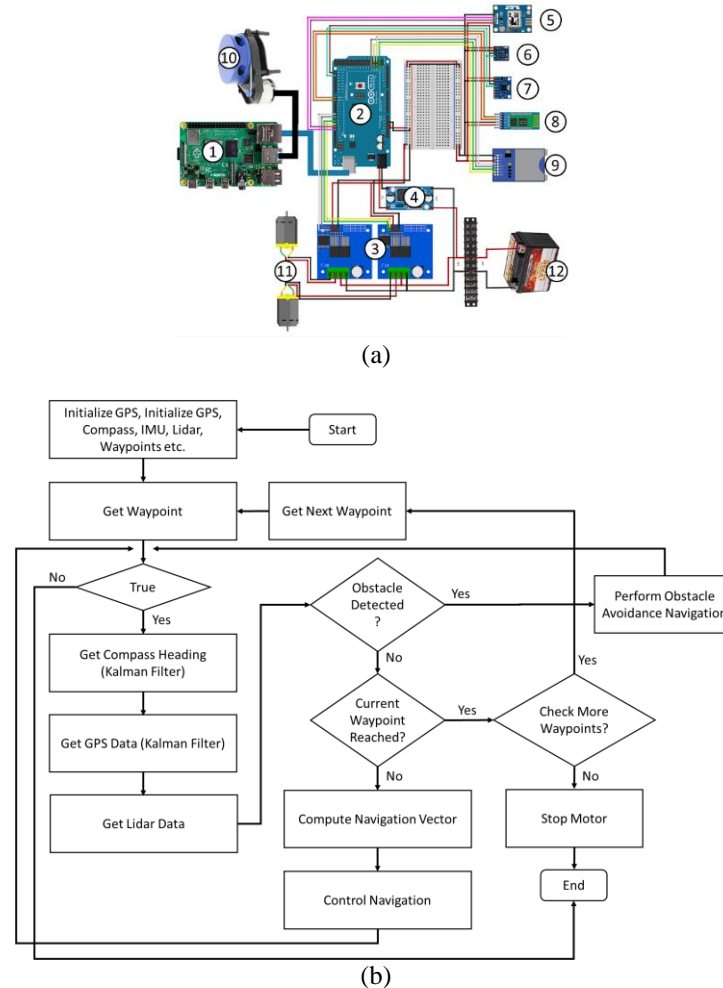


Figure 3. Electronics and software design (a) wiring diagram and (b) flowchart system

2.3. Evaluation

Figure 4 presents the experimental coordinates and their corresponding details, providing a comprehensive overview of the setup. Field testing is done to assess this mobile robot's readiness at the coordinates 14.0345936,100.7333836, as shown in Figure 4(a). The waypoint paths in the testing scenario are categorized into three shapes: triangle, square, and rectangle. The target pathways in Figures 4(b) to 4(d) show several waypoints, each of which represents a different trajectory that the robot must follow. These field tests evaluate the robot's capabilities and performance in various path configurations, offering important information about its operational efficacy and possible areas for development. The data from the compass sensor, GPS, and Kalman filter results are then recorded. These results are then evaluated using formula root mean square percentage error (RMSPE) (14) to test the accuracy level of the sensors and Kalman Filter compared to the given target waypoints [31].

$$RMSPE = \frac{\sqrt{\frac{1}{N} \sum_{i=1}^N (y_i - \hat{y}_i)^2}}{Mean(y)} \times 100 \tag{14}$$

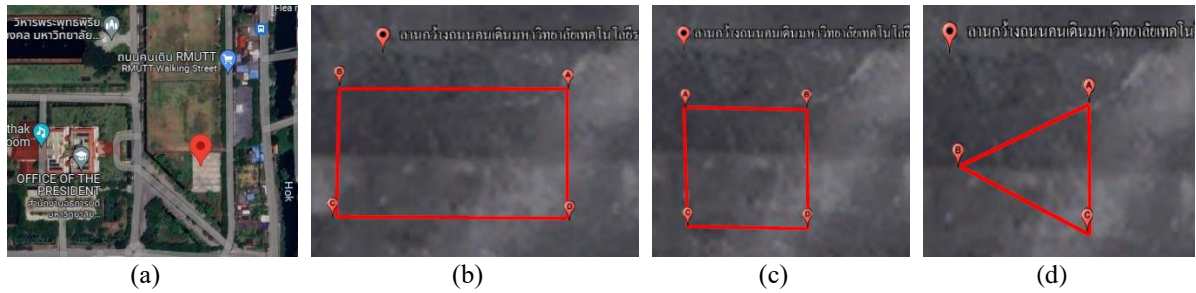


Figure 4. The experimental coordinates and scenario for: (a) location (b) rectangle, (c) square, and (d) triangle waypoints

3. RESULTS AND DISCUSSION

3.1. Mechanical and electronics assembly

This section discusses the mechanical design assembly of the Armoured mobile robot. The creation of this robot is based on pre-made CAD designs. Figure 5 presents the outline of the hardware/mechanics that have been made. Figures 5(a) and 5(b) show the side and top views of the robot. It can be seen that the tank body, tank top cover, bearing wheel, rear driving wheel, coil spring, strut, lower roll, metal track, and metal chains are already installed on the two right and left sides of the robot. Figures 5(c) and 5(d) present a series of electronics connected to each other to create the navigation control for the Armoured mobile robot. The DC motor is located at the back of the robot as the prime mover.

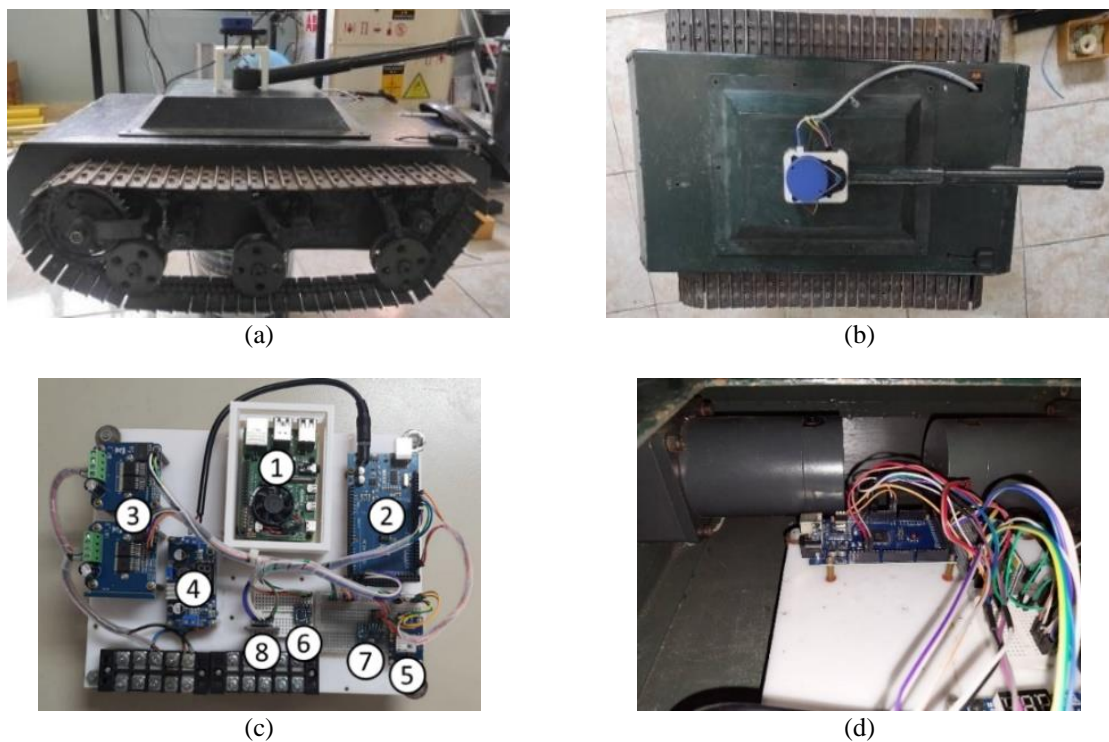


Figure 5. AMR implementation in the: (a) side view, (b) top view, (c) electronics component, and (d) DC motors installation

3.2. Software deployment and field test

The kinematic model of the AMR with tracked wheels was then validated by applying the formula to the simulation. The simulation was carried out by following three scenarios, namely waypoints in the form of triangles, squares, and rectangles. These scenarios consist of geometric shapes defined by sets of waypoints and corresponding completion times. The results of the simulation are presented in Figure 6,

where Figure 6(a) represents a simulation with triangular waypoints, Figure 6(b) with square waypoints, and Figure 6(c) with rectangular waypoints. In addition to tracking and following the given points, the simulation also included an obstacle in the form of a square-shaped pixel. By incorporating a lidar sensor, the robot managed to navigate evasively and maintain effective tracking in all three scenarios. The triangular scenario is defined by the waypoints [10 5; 30 5; 20 17.5; 10 5] and takes 70 seconds to complete. In the square scenario, the waypoints [13 5; 23 5; 23 15; 13 15; 13 5] outline the shape, with a completion time set at 52 seconds. The rectangle scenario, defined by waypoints [10 5; 25 5; 25 15; 10 15; 10 5], requires 66 seconds to complete. These scenarios likely serve as navigation or movement challenges where participants or systems traverse the specified waypoints within the allocated time frames.

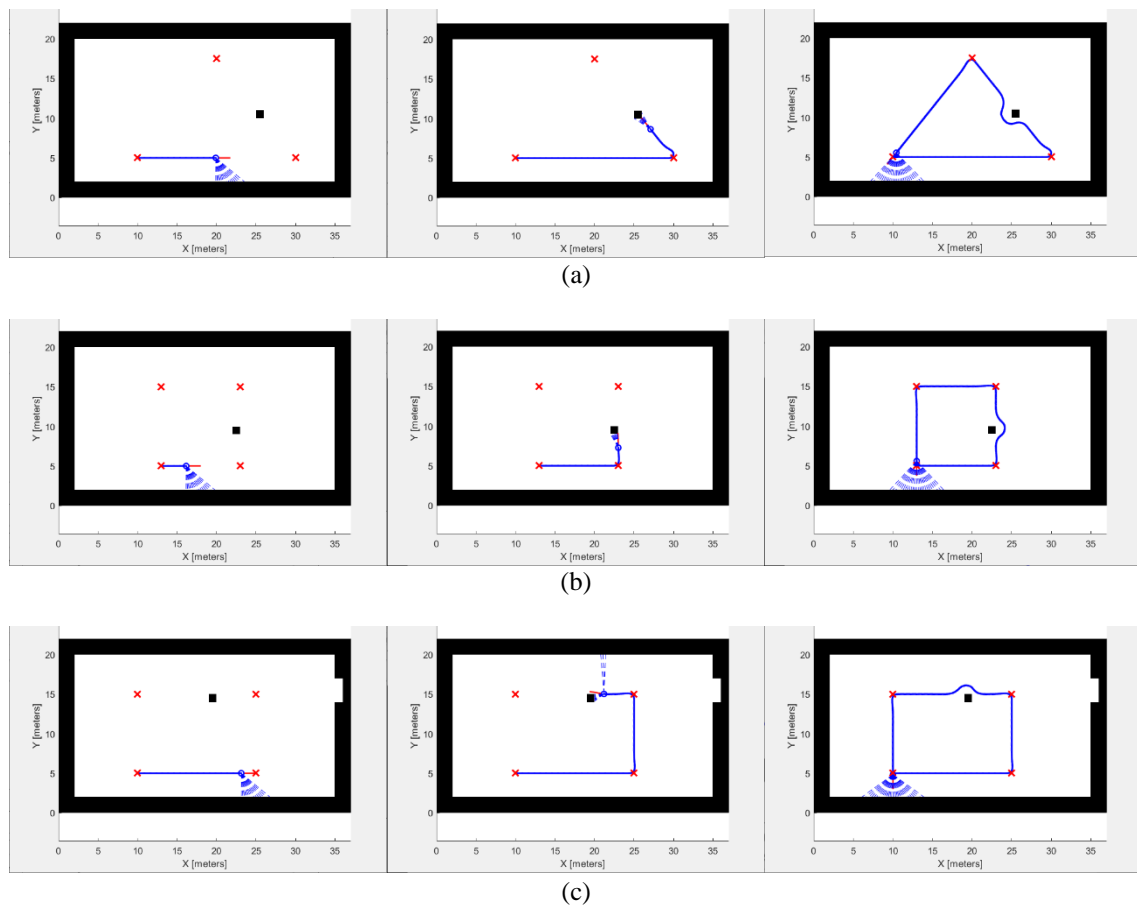


Figure 6. Waypoint simulation: (a) triangle, (b) square, and (c) rectangle

After the simulation is complete, the waypoint algorithm is embedded in the AMR. The Figure 7 shows experimental results showcasing obstacle avoidance techniques utilizing Lidar readings. It presents visualizations from three distinct scenarios: in Figure 7(a) wired obstacle detection, likely utilizing sensors connected via wires; Figure 7(b) indoor Lidar reading visualization, demonstrating obstacle perception within indoor environments; and Figure 7(c) outdoor Lidar reading visualization, illustrating obstacle interpretation in outdoor settings.

As a result of field testing, compass and GPS data were recorded and compared between target waypoint values, sensor values, and sensor values to which the Kalman filter had been applied. The experimental results comparing various scenarios using GPS sensor readings and Kalman-filtered GPS data, presented through visualizations as shown in Figure 8. It outlines comparisons between raw GPS sensor readings and Kalman-filtered GPS data for square, rectangular, and triangular paths. Specifically, it shows the Figure 8(a) squared GPS sensor reading, Figure 8(b) squared GPS Kalman filtered, Figure 8(c) rectangular GPS sensor reading, Figure 8(d) rectangular GPS Kalman filtered, Figure 8(e) triangular GPS sensor reading, and Figure 8(f) triangular GPS Kalman filtered. In each scenario, two obstacles are provided, and the robot is able to navigate, avoiding and following the given waypoints. Meanwhile, experimental

results are shown in Figure 9, which compares compass sensor readings in the square in Figure 9(a), rectangle in Figure 9(b), and triangle in Figure 9(c) scenarios before and after applying a Kalman filter. The comparison provides information about how well the filter works to increase accuracy and dependability. These situations, which are likely to vary in complexity, enable evaluation of the filter's capacity to reduce noise and mistakes in sensor data, improving the robot's navigation accuracy.

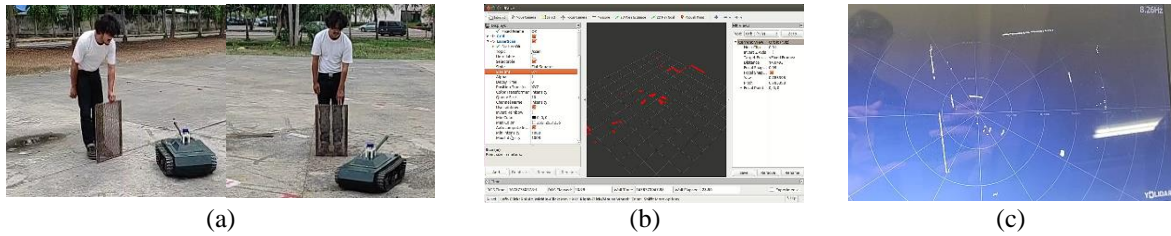


Figure 7. Obstacle avoidance using lidar: (a) wired obstacle, (b) indoor, and (c) outdoor visualization

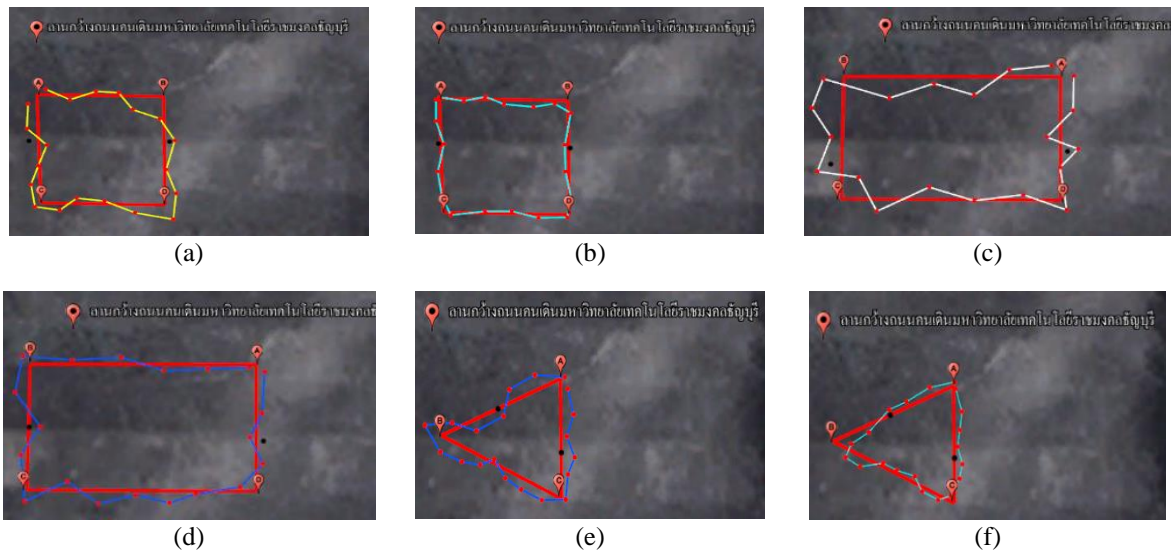


Figure 8. Experimental results visualisation of all scenarios comparing: (a) squared GPS sensor reading, (b) squared GPS kalman filtered, (c) rectangle GPS sensor reading, (d) rectangle GPS kalman filtered, (e) triangle GPS sensor reading, and (f) triangle GPS kalman filtered

Table 2 presents RMSPE values for GPS sensor readings and Kalman filtered GPS data, as well as Kalman filtered compass data, across different geometric scenarios. For the square scenario, the GPS sensor RMSPE is 1.02559, while the GPS Kalman RMSPE is slightly higher at 1.35922, indicating a slight increase in error after Kalman filtering. However, the compass Kalman RMSPE is considerably higher at 8.26708, suggesting significant error in compass data after Kalman filtering. In the rectangle scenario, both GPS sensor and Kalman RMSPE values are higher compared to the square scenario, with GPS sensor RMSPE at 2.91329 and GPS Kalman RMSPE at 2.66248. The compass Kalman RMSPE decreases notably to 1.82381 in this scenario. Finally, in the triangle scenario, the GPS sensor RMSPE is highest at 8.54065, but it decreases significantly to 1.03170 after Kalman filtering, indicating substantial error reduction. The compass Kalman RMSPE for the triangle scenario is 4.94345, indicating moderate error reduction compared to the GPS Kalman RMSPE. Overall, these results suggest varying levels of error reduction achieved through Kalman filtering across different geometric scenarios, with notable improvements observed particularly in GPS data accuracy. The results emphasise the advantages of the suggested system, including its capacity to ensure precise navigation even when impediments are present. Nevertheless, the presence of elevated RMSPE values in specific cases indicates the need for enhancements, such as the optimisation of sensor fusion techniques and the fine-tuning of the Kalman filter parameters. The study's results align with prior

research but provide notable improvements in practical usefulness, especially in intricate settings where conventional approaches may be inadequate.

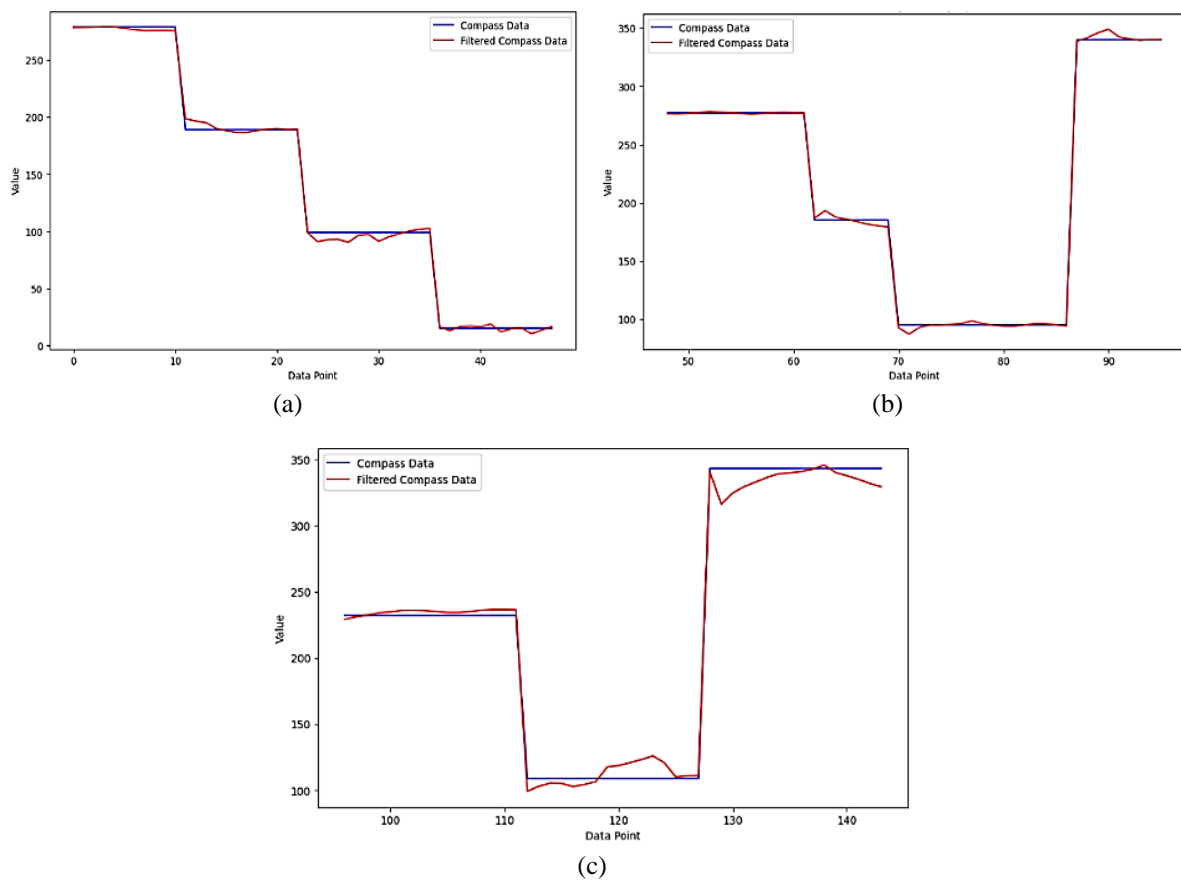


Figure 9. Experimental results comparing compass sensor Kalman filtered reading using: (a) square, (b) rectangle, and (c) triangle scenarios

Table 2. Kalman filter performance

Scenario	GPS sensor RMSPE	GPS Kalman RMSPE	Compass Kalman RMSPE
Square	1.02559	1.35922	8.26708
Rectangle	2.91329	2.66248	1.82381
Triangle	8.54065	1.03170	4.94345

4. CONCLUSION

The complex details of developing, putting into practice, and testing the Armoured mobile robot have all been covered in this paper, with special attention paid to the robot's mechanical layout, navigational algorithms, and sensor integration. The effectiveness and functionality of the robot's navigation system have been closely examined and assessed via stringent field testing and simulations. The outcomes of the simulations and field testing have given important new information on the capabilities and constraints of the armoured mobile robot. The robot has proven to be proficient at navigating a variety of situations and successfully avoiding obstacles, as evidenced by the successful validation of its navigation algorithms, especially the integration of GPS, Lidar, and Kalman filtering. The experimental data has demonstrated the importance of sophisticated signal processing methods in improving the navigation accuracy and reliability. The Armoured mobile robot has also demonstrated its versatility and adaptability by successfully completing predetermined pathways and obstacle avoidance maneuvers, as well as by navigating a variety of terrains and complicated settings. These accomplishments demonstrate the robot's potential for use in real-world applications, such as industrial automation and search and rescue operations. In order to further advance the capabilities and applicability of the Armoured mobile robot in a variety of environments and tasks, future work could concentrate on improving sensor fusion techniques to improve perception accuracy,

implementing autonomous decision-making algorithms for dynamic path planning, integrating machine learning and AI for adaptive navigation strategies, enhancing energy efficiency and durability for long-term autonomy, and investigating ways to improve human-robot interaction.

ACKNOWLEDGEMENTS

The Department of Mechatronics Engineering at Rajamangala University of Technology Thanyaburi, in particular, has provided the authors with essential help and resources during this research. The authors would like also to express their gratitude to every one of the instructors, staff, and students who helped make this project possible.

REFERENCES

- [1] P. Kraipornsak, "Good governance and economic growth: an investigation of Thailand and selected Asian countries," *Eurasian Journal of Economics and Finance*, vol. 6, no. 1, pp. 93–106, 2018, doi: 10.15604/ejef.2018.06.01.009.
- [2] C. Yamahata, D. M. Seekins, and M. Takeda, *Social Transformations in India, Myanmar, and Thailand: volume i social, political and ecological perspectives*. 2021.
- [3] A. B. Rashid, A. K. Kausik, A. A. H. Sunny, and M. H. Bappy, "Artificial intelligence in the military: an overview of the capabilities, applications, and challenges," *International Journal of Intelligent Systems*, vol. 2023. Wiley-Hindawi, 2023, doi: 10.1155/2023/8676366.
- [4] D. Patil, M. Ansari, D. Tendulkar, R. Bhatlekar, V. N. Pawar, and S. Aswale, "A survey on autonomous military service robot," in *International Conference on Emerging Trends in Information Technology and Engineering, ic-ETITE 2020*, Institute of Electrical and Electronics Engineers Inc., Feb. 2020, doi: 10.1109/ic-ETITE47903.2020.78.
- [5] Q. P. Ha, L. Yen, and C. Balaguer, "Robotic autonomous systems for earthmoving in military applications," *Automation in Construction*, vol. 107. Elsevier B.V., Nov. 01, 2019, doi: 10.1016/j.autcon.2019.102934.
- [6] M. Cooney, M. Shiomi, E. K. Duarte, and A. Vinel, "A broad view on robot self-defense: rapid scoping review and cultural comparison," *Robotics*, vol. 12, no. 2, Apr. 2023, doi: 10.3390/robotics12020043.
- [7] C. Mavrogiannis *et al.*, "Core challenges of social robot navigation: a survey," *ACM Trans Hum Robot Interact*, vol. 12, no. 3, Apr. 2023, doi: 10.1145/3583741.
- [8] W. Puriwat and S. Tripopsakul, "Preparing for Industry 4.0-will youths have enough essential skills?: An evidence from Thailand," *International Journal of Instruction*, vol. 13, no. 3, pp. 89–104, Jul. 2020, doi: 10.29333/iji.2020.1337a.
- [9] R. Pillai, A. G. Banerjee, and S. K. Gupta, "A heterogeneous robots collaboration for safety, security, and rescue robotics: design, architecture, and algorithms," *Robotics and Autonomous Systems*, vol. 38, no. 3, pp. 129–151, Feb. 01, 2024, doi: 10.1080/01691864.2024.2309622.
- [10] W. Budiharto, E. Irwansyah, J. S. Suroso, and A. A. S. Gunawan, "Design of object tracking for military robot using pid controller and computer vision," *ICIC Express Letters*, vol. 14, no. 3, pp. 289–294, 2020, doi: 10.24507/icicel.14.03.289.
- [11] C. G. Pachón-Suescún, C. J. Enciso-Aragón, and R. Jiménez-Moreno, "Robotic navigation algorithm with machine vision," *International Journal of Electrical and Computer Engineering*, vol. 10, no. 2, pp. 1308–1316, 2020, doi: 10.11591/ijece.v10i2.pp1308-1316.
- [12] M. Javaid, A. Haleem, R. P. Singh, and R. Suman, "Substantial capabilities of robotics in enhancing industry 4.0 implementation," *Cognitive Robotics*, vol. 1. KeAi Communications Co., pp. 58–75, Jan. 01, 2021, doi: 10.1016/j.cogr.2021.06.001.
- [13] P. N. Crisnapati, D. Maneetham, and E. Triandini, "Trolls: a novel low-cost controlling system platform for walk-behind tractor," *International Journal of Electrical and Computer Engineering*, vol. 13, no. 1, pp. 842–858, 2023, doi: 10.11591/ijece.v13i1.pp842-858.
- [14] P. N. Crisnapati and D. Maneetham, "Two-dimensional path planning platform for autonomous walk behind hand tractor," *Agriculture (Switzerland)*, vol. 12, no. 12, Dec. 2022, doi: 10.3390/agriculture12122051.
- [15] I. N. Kitashvili, "Application of synoptic magnetograms for prediction of solar activity using ensemble kalman filter," 2019.
- [16] T. Wu and J. Y. Hung, "State estimation for a tractor-trailer system using adaptive unscented Kalman filter," in *Conference Proceedings IEEE Southeastcon*, Institute of Electrical and Electronics Engineers, 2017, doi: 10.1109/SECON.2017.7925342.
- [17] H. A. Jeyed and A. Ghaffari, "Nonlinear estimator design based on extended Kalman filter approach for state estimation of articulated heavy vehicle," *Proceedings of the Institution of Mechanical Engineers, Part K: Journal of Multi-body Dynamics*, vol. 233, no. 2, pp. 254–265, Jun. 2019, doi: 10.1177/1464419318772173.
- [18] M. Wickert and C. Siddappa, "Exploring the extended Kalman filter for GPS positioning using simulated user and satellite track data," *In SciPy*, pp. 84–90, 2018.
- [19] J. Patoliya, H. Mewada, M. Hassaballah, M. A. Khan, and S. Kadry, "A robust autonomous navigation and mapping system based on GPS and LiDAR data for unconstrained environment," *Earth Science Informatics*, vol. 15, no. 4, pp. 2703–2715, Dec. 2022, doi: 10.1007/s12145-022-00791-x.
- [20] S. Zhou *et al.*, "Robust path following of the tractor-trailers system in GPS-denied environments," *IEEE Robotica Automatica Letters*, vol. 5, no. 2, pp. 500–507, Apr. 2020, doi: 10.1109/LRA.2019.2956380.
- [21] Z. Zhang, "Path planning of a firefighting robot prototype using GPS navigation," in *ACM International Conference Proceeding Series*, Association for Computing Machinery, Jun. 2020, pp. 16–20, doi: 10.1145/3402597.3402612.
- [22] R. N. Jazar, *Theory of applied robotics: kinematics, dynamics, and control, second edition*, Second Edition. Springer Science and Business Media., 2010.
- [23] J. L. Martínez, A. Mandow, J. Morales, S. Pedraza, and A. García-Cerezo, "Approximating kinematics for tracked mobile robots," *International Journal of Robotics Research*, vol. 24, no. 10, pp. 867–878, Oct. 2005, doi: 10.1177/0278364905058239.
- [24] N. Strawa, D. I. Ignatyev, A. C. Zolotas, and A. Tsourdos, "On-line learning and updating unmanned tracked vehicle dynamics," *Electronics (Switzerland)*, vol. 10, no. 2, pp. 1–38, Jan. 2021, doi: 10.3390/electronics10020187.
- [25] J. Taghia and J. Katupitiya, *Springer Tracts in Advanced Robotics 138 Applied Guidance Methodologies for Off-road Vehicles*, vol. 138. 2020, [Online]. Available: <http://www.springer.com/series/5208>.
- [26] D. Maneetham, P. N. Crisnapati, and Y. Thwe, "Autonomous open-source electric wheelchair platform with internet-of-things and proportional-integral-derivative control," *International Journal of Electrical and Computer Engineering*, vol. 13, no. 6, pp. 6764–6777, Dec. 2023, doi: 10.11591/ijece.v13i6.pp6764-6777.

- [27] W. Li, J. Guo, L. Ding, J. Wang, H. Gao, and Z. Deng, "Teleoperation of wheeled mobile robot with dynamic longitudinal slippage," *IEEE Transactions on Control Systems Technology*, vol. 31, no. 1, pp. 99–113, Jan. 2023, doi: 10.1109/TCST.2022.3174773.
- [28] M. F. Cakir, S. Sezer, and M. Bayraktar, "Modeling and simulation of elevation dynamics of main battle tank weapon system with linear graph method," *Arabian Journal for Science and Engineering*, 2024, doi: 10.1007/s13369-023-08546-6.
- [29] G. Yamauchi, K. Nagatani, T. Hashimoto, and K. Fujino, "Slip-compensated odometry for tracked vehicle on loose and weak slope," *ROBOMECH Journal*, vol. 4, no. 1, Dec. 2017, doi: 10.1186/s40648-017-0095-1.
- [30] X. Wang, J. Taghia, and J. Katupitiya, "Robust model predictive control for path tracking of a tracked vehicle with a steerable trailer in the presence of slip," in *IFAC-PapersOnLine*, Elsevier B.V., 2016, pp. 469–474, doi: 10.1016/j.ifacol.2016.10.085.
- [31] J. Krohkaew, P. Nilaphruek, N. Witthayawiroj, S. Uapipatanakul, Y. Thwe, and P. N. Crisnapati, "Thailand raw water quality dataset analysis and evaluation," *Data (Basel)*, vol. 8, no. 9, Sep. 2023, doi: 10.3390/data8090141.

BIOGRAPHIES OF AUTHORS



Tanya Porang    presently, Colonel Tanya Porang is employed by the esteemed Chulachomklat Royal Military Academy as a Physics Instructor. He offers a variety of knowledge to his position and has a strong interest in military research, particularly in Unmanned Armored Vehicle System Technology. Because of his expertise in Next-Generation Automotive Technology, he is able to lead innovation and make a substantial impact on the development of military vehicle technology. He is currently pursuing a doctorate degree at RMUTT's Mechatronics Engineering Department in an effort to achieve even greater academic success. His pursuit of this academic goal is evidence of his enthusiasm for lifelong learning and the advancement of military technology expertise. He can be contacted at email: tanya_p@mail.rmutt.ac.th.



Dechrit Maneetham    currently serves as an Associate Professor in Mechatronics Engineering at Rajamangala University of Technology in Thanyaburi, Thailand. His academic journey includes earning B.Ind.Tech. in Material Handling Technology and M.S. in Mechanical Engineering from King Mongkut's University of Technology in North Bangkok. In 2010, he achieved a D.Eng. in Mechatronics from the Asian Institute of Technology, followed by a Ph.D. in Electrical and Computer Engineering from Mahasarakham University in 2018. With a wealth of experience exceeding 15 years in teaching engineering, he has significantly contributed to the field. His contributions extend to the publication of over 85 technical papers. Beyond academia, he has shared his knowledge through robotics short courses at various conferences and authored seven books. He can be contacted at email: dechrit_m@rmutt.ac.th.



Padma Nyoman Crisnapati    earned his bachelor's degree in 2009 from the Department of Informatics Engineering at Sepuluh Nopember Institute of Technology. Subsequently, he pursued a master's degree in Learning Technology in 2011 and another master's degree in Computer Science in 2018, both from Ganesha Education University. He successfully earned a D.Eng. in the Mechatronics Engineering Department at Rajamangala University of Technology Thanyaburi (RMUTT). His diverse research interests encompass various domains, including mechatronics, robotics, automation, augmented and virtual reality, 2D and 3D animation, and internet of things. He can be contacted at email: crisnapati@rmutt.ac.th.